A novel multi-molecular catalysis for CO_2 decomposition

Karthika devi & Chellapandiankannan*
Department of Chemistry, Manonmaniam Sundaranar University, Abishekapatti
Tirunelveli-627012, Tamil Nadu, India.
* E-mail: chellapandiankannan@gmail.com, ORCID: 0000-0002-6244-8367

Abstract

The CO_2 decomposition is needed high temperature in conventional methods. Our aim is to reduce the CO_2 decomposition temperature. In this view **multi-molecular catalysis** is essential. It is achieved through Multiple catalytic sites. The Multiple catalytic sites are created through a **novel intercrossing framework** catalyst. The intercrossing framework is created between MgO framework and $AlPO_4$ framework by the template (TPAOH). The catalyst has multiple acidic sites on superoxide ion, oxyanion, octahedral Al^{3+} and Mg^{2+}. The intercrossing frameworks is achieved in first time and the material is named as **Kankarlite-2**. The active sites and intercrossed framework are confirmed in the crystal structure drawn by XRD data. The surface area is $60m^2/g$ and pore volume is $2.9cm^3/g$. The TGA and TEM analysis are the supportive evidence for the intercrossing of the two frameworks. Though the surface area and pore volume is low, the activity is too high due to the intercrossing framework. The effective catalytic activity at lower temperature may be due to the **cooperative effect** of such multiple active sites which leads to the **multi-molecular assembling** of CO_2 molecules. This assembling reduces the **CO_2 decomposition temperature (63%)**. The multi-molecular assembling is calculated by a new formula of $P_n = R\frac{mT}{Wt}$. Thus we have achieved intercrossing framework catalyst and multi-molecular catalysis for Carbon capturing at lower temperature.

KEYWORDS

Intercrossed framework, multiple acidic sites, multi-molecular catalysis, CO_2 decomposition

1. Introduction

Global warming is an international issue [1] and the most important anthropogenic greenhouse gas contributing to the enhanced greenhouse effect both presently and in the foreseeable future is CO_2 [2]. The combustion of most carbon-containing substances produces CO_2 [3]. Several technologies are available for CO_2 capture, including chemical absorption, membrane separation, adsorption and cryogenic CO_2 capture. The traditional method of absorption by liquid amines [4], ionic liquids [5], amino acid-functionalized ionic liquid [6], ionic-mixed solvents [7] and deep eutectic solvents [8] are promising materials. Yet, despite their advantages, they suffer from serious corrosion problems, considerable energy loss, high sorbent cost, lower gas–liquid interfacial surface area and ineffective regeneration [9]. As a result of these limitations, CO_2 adsorption using solid porous materials especially aluminophosphate materials offers several advantages, including enhanced uptake efficiency, simple recovery, high adsorption capacity even in humid conditions, ease of handling and material stability [10]. Generally, the $AlPO_4$ materials are microporous in nature, which restricts the incorporation of large organic molecules into their pores. Their limited pore size hinders their practicality in catalyzing reactions involving large molecules. In order to overcome this limitation and enhance the pore size of $AlPO_4$ materials, numerous research groups have undertaken efforts to create mesoporous molecular sieves [11]. Mesoporous $AlPO_4$ molecular sieves are typically synthesized using the conventional hydrothermal method [12]. This involves crystallizing an active aqueous aluminophosphate gel that contains templating agents like organic amines or quaternary ammonium ions [13]. But the disadvantage of this method is that the process has taken a long time [14] and also requires high temperature [15]. The reaction had been carried out in an autoclave. So there is some necessity to overcome such issues. In this paper, we have explored the room temperature synthesis of MgO-

$AlPO_4$ catalyst with intercrossing frameworks using the simple Sol gel method in a short period of time compared to the synthesis process in reported literature [16]. Isomorphously substituted Mg-$AlPO_4$ has been reported in the literature by CTAB [16], di-n-propyleneamine [17] etc without autoclave. But the framework intercrossing in MgO-$AlPO_4$ has not yet been reported. The term intercrossing means two different frameworks are intercrossed together, creating a single structure with unique properties [18] [19]. There are only a few reports about intercrossing framework in carbon nanotubes [20] and polymers [21]. As of now, there is no report on the intercrossing framework in mesoporous and microporous molecular sieves. Thus the synthesized MgO-$AlPO_4$ is applied for CO_2 decomposition. In the reported literature, n-butylamine templated isomorphous substituted Mg-$AlPO_4$ was used as a catalyst for CO_2 decomposition. Though employing the same CO_2 decomposition method as in the present study, the achieved oxygen selectivity was only 50% [22]. So to attain higher oxygen selectivity, a novel intercrossed framework of MgO-$AlPO_4$ is synthesized and applied for CO_2 decomposition. The framework creates multiple acidic sites which are useful to reduce CO_2 decomposition activation energy and hence the reaction may be possible at lower temperature with high O_2 selectivity.

2. Experimental

2.1 Materials

The following materials are used as a source for the synthesis of MgO-$AlPO_4$: Aluminium hydroxide (Merck), Orthophosphoric acid (Nice, GR), Magnesium sulphate (Merck,GR) and Tetrapropylammonium hydroxide (99% purity, Lobal Chemie). All these chemicals are used in the synthesis without further treatment.

2.2 Synthesis of $MgO\text{-}AlPO_4$

$MgO\text{-}AlPO_4$ is prepared by implementing the sol-gel method with the molar composition of the gel is $Al(OH)_3$: H_3PO_4 : TPAOH : 0.05 $MgSO_4$: $13.8H_2O$. About 7.8g of aluminium hydroxide is mixed in 100ml of deionized water and 20ml of TPAOH is dissolved in 50ml of water. The two solutions are combined and stirred for one hour at room temperature using a magnetic stirrer. Following that, approximately 5.8ml of orthophosphoric acid and 6g of magnesium sulphate are added to the mixture, which is continuously stirred for 2 hours to obtain a homogeneous mixture. The resulting mixture is kept undisturbed for 16 hours for crystallization. Then the supernatant liquid is decanted and the settled precipitate is washed thoroughly with deionized water until the pH becomes neutral. The precipitate is then dried at 200°C in a hot oven, followed by calcination at 400°C for 5 hours to remove the template molecules from the pores.

2.3 Catalytic reactor

The catalytic reaction is performed through a U-shaped tube filled with calcined catalyst, both sides of the U-shaped reactor are packed with asbestos wool. It is immersed in engine oil to maintain the temperature. The engine oil beaker is placed on a hot plate. The inlet of the reactor is connected to a cylinder and the outlet is connected to a gas collector. The CO_2 gas is allowed to flow through the reactor. The product is collected in a gas collector.

2.4 Gas Chromatography analysis

The efficiency of the decomposition process is analyzed by a Shimadzu chromatograph equipped with a thermal conductivity detector and packed column. Chromatographic conditions are maintained at 5 V and a current of 115 mA. The analysis is conducted by collecting the final gas product every hour to optimize the temperature, flow rate, catalyst dosage and time on stream.

2.5 Characterization techniques

The crystal structure of the materials is characterised by X-ray powder diffraction patterns in the 2θ range of 5° - 80° with the use of Bruker, an advanced D8 X-ray diffractometer with Cu-Kα radiation. Fourier transform infrared (FTIR) spectra are recorded by the FT-IR 8400S (Shimadzu) spectrometer. The samples were pressed into a pellet with KBr. It is analyzed in the wavelength domain of 400 – 4000 cm^{-1}. The Brunauer-Emmett-Teller (BET) surface area measurements are carried out by micrometrics ASAP2010 instrument. The samples were previously outgassed for 30 minutes at 150°C and then heated for 120 minutes at 350°C. N_2 adsorption and desorption are recorded at 77K. Static chemisorption is carried out with the Quantachrome autosorb iq instrument. About 0.112g sample is packed in the bed and degassed with Helium gas at 150°C for 2 hours. The adsorption of ammonia gas has been carried at 40°C and desorbed at 400°C for 35minutes. High-resolution transmission electron microscopy (HR-TEM) images are taken by the JEOL JEM 2100 (200 kV). Dropping a colloidal solution over carbon-coated copper grids yielded the samples. This microscope enables to view lattice resolution of 0.14 nm and point-to-point resolution of 0.19 nm.

3. Result and Discussion

3.1 XRD Analysis

The XRD analysis of MgO-$AlPO_4$ has been carried out from 2θ range of 5 to 80º. It is shown in Figure 1. The peaks at 8.86°, 16.2° and 21.29° are indexed to (110), (301) and (512) planes are resembled that the crystal system of $AlPO_4$ is triclinic (match file - 96-101-0142 and unit cell parameters are a=6.13, b=7.51, c=8.58). The d-spacing and the peaks at 38.2°, 44.5°,66.8° and 78.2° are indexed to (111), (200), (202) and (311) planes which are

resembled that the crystal system of Mg-O is cubic phase. These peaks are good in agreement with the match file- 96-901-3253 and the unit cell parameters are a=b=c= 3.97.

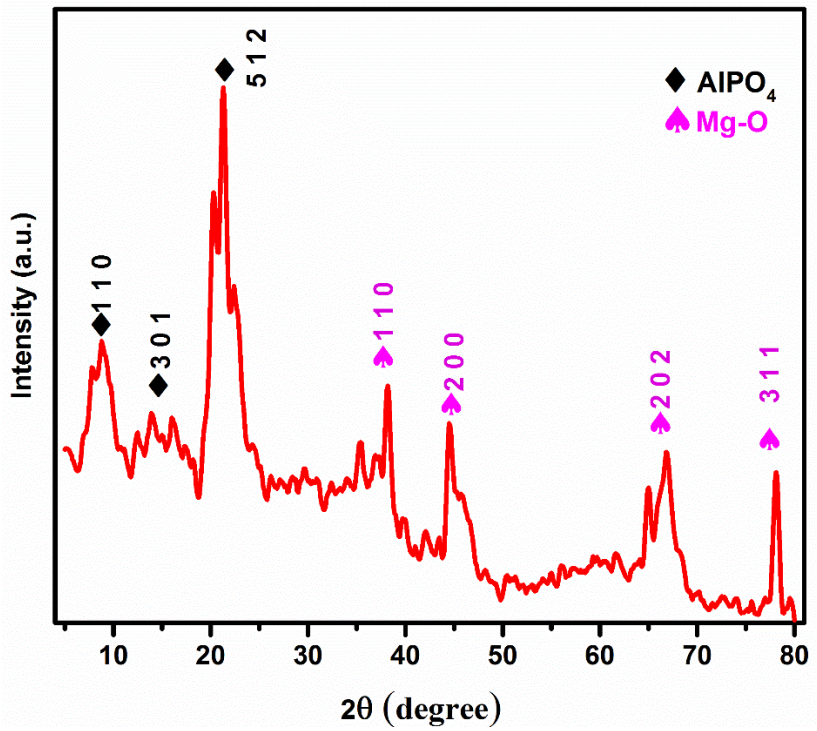

Figure 1. XRD pattern of MgO-$AlPO_4$

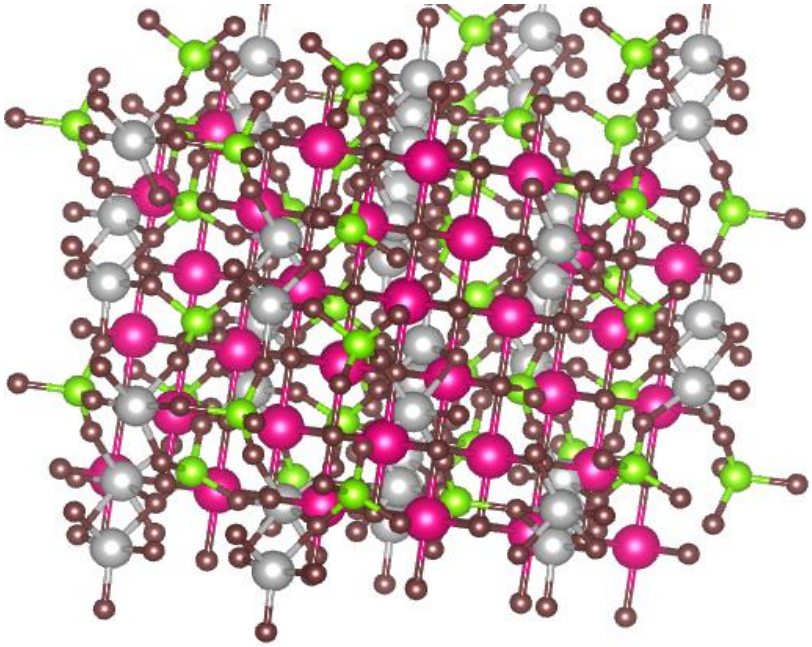

Silverish grey- Aluminium, Green- Phosphorous, Brown- Oxygen, Pink- Magnesium

Figure 2. Crystal structure – intercrossing of MgO and $AlPO_4$ framework

From Figure 2, it is clearly observed that the two frameworks of MgO and $AlPO_4$ are formed as a single material. The magnesium atoms are linked through tetragonal oxygen, which is formed superoxide ions (O^{2-}). The MgO has an octahedral framework. In $AlPO_4$ octahedral aluminium (AlO_6) is connected with tetragonal phosphate through tri-coordinate oxygen and form oxyanions (O^-). When compared to reported XRD pattern of MgO and $AlPO_4$ with the intercrossed framework of MgO and $AlPO_4$, three important changes are observed in the XRD pattern. 1. a new peak is emerged at 8.8°, 2. The shifting in the 2θ values of intercrossed framework of MgO and $AlPO_4$ and 3. All peaks are splitted in the intercrossed framework of MgO and $AlPO_4$ compared to reported XRD patterns of MgO and $AlPO_4$ [23]. These three evidences are proved the intercrossing frameworks of MgO and $AlPO_4$.

Intercrossing of framework

The MgO framework and $AlPO_4$ framework are intercrossed between them. It may be due to the H^+ ion released from H_3PO_4 which is reacted with $Mg(OH)_2$ to produce MgO framework. The formed phosphate ion induces the $AlPO_4$ framework. Ultimately, the phosphoric acid induces both the frameworks and so the intercrossing of the two frameworks happens (Figure 2).

3.2 Proposed mechanism for Superoxide ion and octahedral Mg catalytic site formation

The multiple acidic sites formation is discussed in the following sections 4.2 and 4.3. The superoxide ion formation is confirmed in the crystal structure which is drawn based on XRD pattern (Figure 2). The superoxide ion formation is may be due to the template effect on MgO framework. The template has OH^- group, which can be exchanged with SO_4^{2-} (two template molecules) as shown in Scheme S1. The sulphate ion has coordinated two template molecules

as an ion pair that is acting as a templating agent. The OH^- group reacts with Mg^{2+} to form Magnesium hydroxide (Mg^{2+}-$(OH)_2$. These magnesium hydroxides are condensed together to produce the MgO framework with the superoxide ion (Scheme S1). In the MgO framework, oxygen has four coordination. The two excess negative charges that appear on oxygen act as superoxide ion, which is balanced by two protons. Similarly, the 4 negative charges on Mg^{2+} are balanced by four protons. The H_3PO_4 initiates the $Mg(OH)_2$ condensation reaction. So there is a possibility for the intercrossing of the $AlPO_4$ framework and the MgO framework.

3.3 Oxyanions and octahedral aluminium catalytic site formation

The Oxyanion formation is confirmed by crystal structure drawn on the basis of XRD pattern (Figure 2). In $AlPO_4$ framework, aluminium is in octahedral coordination, it may be due to the template effect, because of the octahedral coordination of aluminium in $AlPO_4$ framework, the oxyanion is formed. The aluminium has three negative charges and oxygen has one negative charge which is balanced by protons as shown in Scheme S2.

3.4 FT-IR Analysis

The FT-IR spectrum of as-prepared and calcinated MgO-$AlPO_4$ are shown in Figure 3. The broad band at 3500 – 3670 cm^{-1} is attributed to the hydroxyl group vibration of Mg-OH, Al-OH groups [24]. An absorption band at 1648 cm^{-1} is due to the N-H bending mode of template molecules [25]. A smaller vibration near 1520 cm^{-1} is owing to the bending mode of water molecules [15]. These three bands are reduced after calcination. The absorption in the region 1100 cm^{-1} is due to asymmetric stretching vibration of the tetrahedral framework [26]. Symmetric stretching vibration of tetrahedral framework or AlO_6 groups is observed at 725 cm^{-1} [27] and 481 cm^{-1} is ascribed to stretching vibration of Mg-O vibration [28] or bending vibrations of P-O in $AlPO_4$ [29]. This is confirmed the presence of magnesium oxide and Aluminophosphate (MgO-$AlPO_4$) framework.

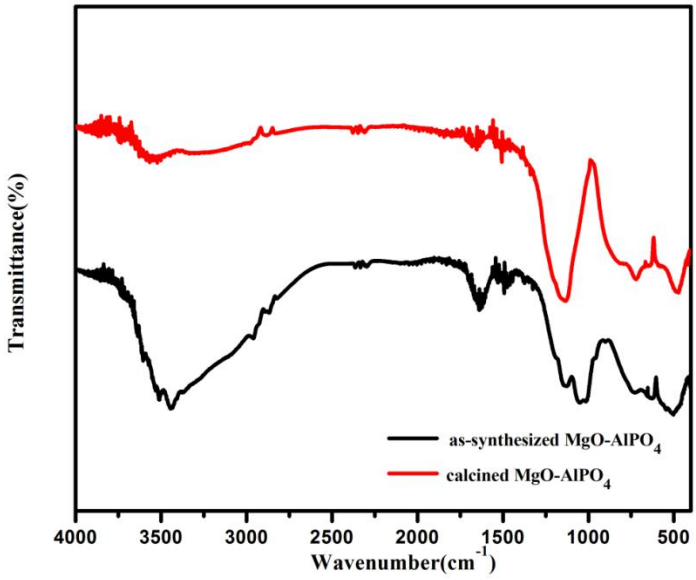

Figure 3. FT-IR Spectra of MgO-$AlPO_4$

3.5 Thermogravimetric Analysis

The thermo–gravimetry analysis (TGA) and differentiation thermo–gravimetric analysis (DTG) curves of MgO-$AlPO_4$ are presented in Figure 4. The TGA curve of MgO-$AlPO_4$ is shown 11.3% weight loss with an exothermic process from 100 to 200°C attributed to the desorption of water [30]. Then 8.46% mass loss between 210 and 325°C assigned to the decomposition of TPAOH [25] and 5.62% mass loss is observed at 450°C, which may be due to the removal of carbon residues. Because the decomposition of TPAOH leaves fewer carbon residues, it may decompose at 450°C [31]. In the reported literature, there is a heavy weight loss of 24% with an endothermic process from 80 to 216°C, which is due to the removal of water along with template molecules. And the second weight loss of 14.06% from 250-310°C is due to the oxidative decomposition of remaining template molecules [32].

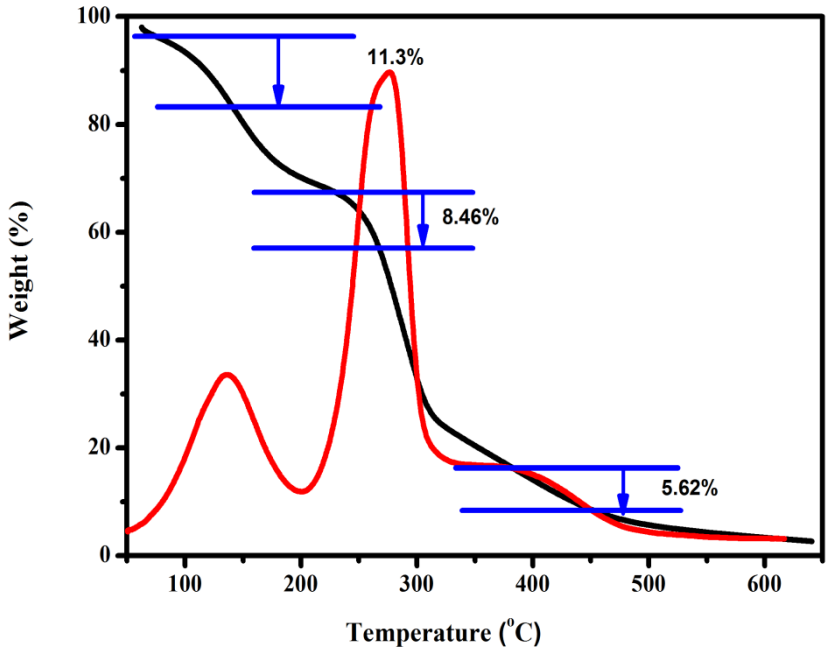

Figure 4. Thermogram of MgO-$AlPO_4$

But in the present study, the weight loss at 450°C is may be due to the intercrossing of $AlPO_4$ and MgO frameworks. The intercrossing may prevent the complete decomposition and desorption of the template from the pore. It results in carbonization. This carbon oxidizes to carbon dioxide at 450°C. The weight loss at 100 to 200°C, 210°C and 325°C are also appeared in the isomorphous substituted Mg^{2+} in the $AlPO_4$ framework [16]. We observed the same weight loss temperature as in isomorphous substituted $MgAlPO_4$. However, the weight loss percentage is reduced in the intercrossing framework of MgO and $AlPO_4$. This may be an evidence for the intercrossing framework of MgO and $AlPO_4$. The intercrossing framework accommodating less quantity of template.

3.6 BET Analysis

The N_2 adsorption–desorption isotherms of the MgO-$AlPO_4$ material is observed in Figure 5 which is indicated that the material has a double pore formation. The corresponding textural properties, such as the BET specific surface area, specific pore volume and average pore diameter are summarized in Table 2.

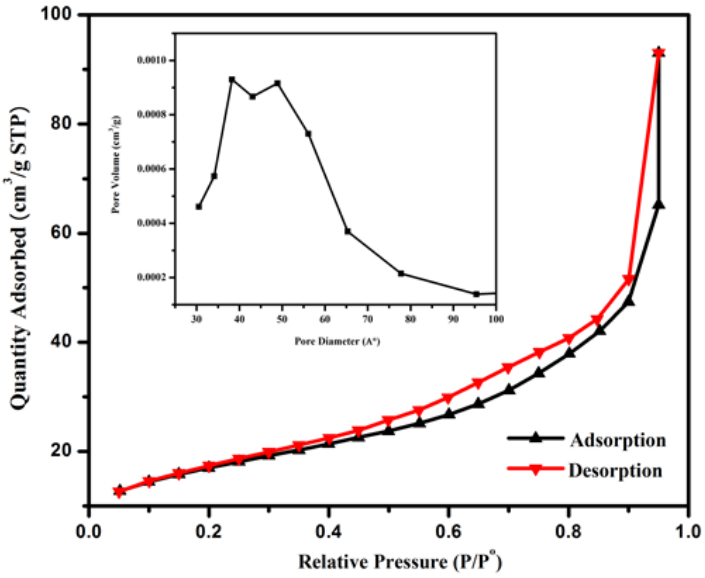

Figure 5.N_2 adsorption isotherm and BJH pore size distribution of $MgO\text{-}AlPO_4$

Table 2 N_2 adsorption isotherm and BJH pore size distribution of $MgO\text{-}AlPO_4$

Catalysts	Surface area (m^2/g)	Pore Diameter (nm)	Pore Volume (cm^3/g)
$MgO\text{-}AlPO_4$	60	4	2.9
		5	

It is clear that the $MgO\text{-}AlPO_4$ has a type-IV isotherm with H1 type hysteresis loop which clearly confirms the mesoporous nature. But the hysteresis loop represents the existence of non-uniform mesopores [33]. This may be due to the two-pore formation in $MgO\text{-}AlPO_4$. In the reported literature, CTAB templated, isomorphous substituted $Mg\text{-}AlPO_4$ has a pore diameter of 2 nm [34]. Similarly, TPAOH templated $Mg\text{-}AlPO_4$ has a pore diameter of 22nm [17]. In the present study, $MgO\text{-}AlPO_4$ has two pore formation (Figure 5). The diameters of two pores are 4 nm and 5nm. It may be due to intercrossing of two frameworks (Figure 2).

3.7 Static chemisorption

The static chemisorption is shown in the Figure 6. The analysis is performed to determine the acid sites in the MgO-$AlPO_4$ catalyst. Ammonia desorbed at 400°C proved that the acid sites are strong. Total ammonia desorption from MgO-$AlPO_4$ is 0.69mmol/g.

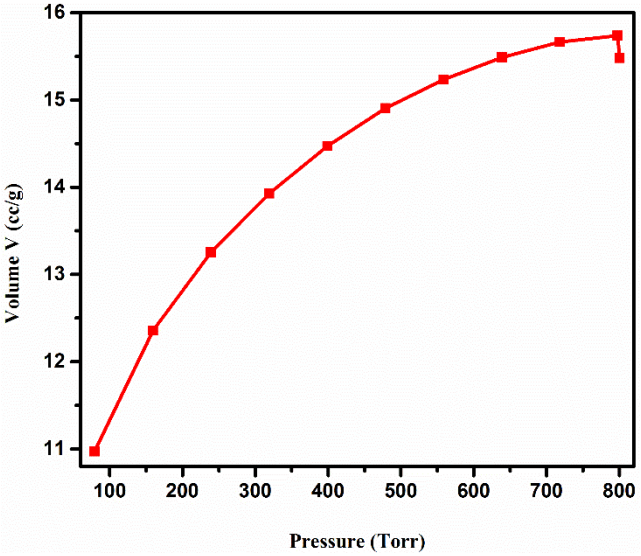

Figure 6. Static chemisorption of MgO-$AlPO_4$

3.8 HR-TEM Analysis

The HR-TEM images of MgO-$AlPO_4$ are shown in Figure S1. The central portion of the particles seems to be thicker than the edges. It is indicated the intercrossing of MgO framework and $AlPO_4$ framework in the center part of the crystal. It is proved by the crystal structure (Figure 2). The presence of bright spots in the SAED pattern is confirmed that the material is polycrystalline in nature [35].

4. Catalytic application of MgO-$AlPO_4$ catalyst

4.1 Effect of Temperature

Catalytic applications have been conducted within a temperature range from room temperature to 250°C. The corresponding data are found in Table S1 and Figure 7.

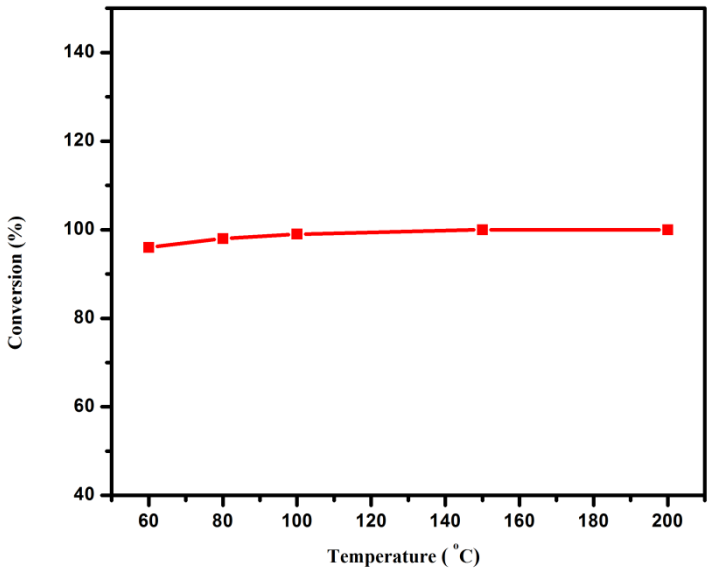

Figure 7. Effect of temperature on CO_2 decomposition over MgO-$AlPO_4$

From Figure 7 and Table S1, it is clearly observed that the conversion and oxygen selectivity are independent of temperature up to 150°C. This is attributed to the enhanced affinity between CO_2 and multiple acidic sites of intercrossed framework of MgO-$AlPO_4$. At 200°C, oxygen selectivity slightly increases (78%) because very weak active sites are also interacting with the CO_2. In general, the CO_2 formation is highly exothermic up to 800°C [36]. But CO_2 decomposition is endothermic reaction [37]. In the conventional method, the catalyst (Zinc exchanged Y zeolite) is required 450°C for CO_2 decomposition with 70% conversion [38]. But in the present investigation, the high conversion and selectivity at 200°C is may be due to the interaction of multiple active sites with CO_2 (octahedral Al and Mg, Superoxide ion and Oxyanion). The CO_2 decomposition temperature is reduced from 450°C to 200°C (63%). The conventional catalyst has no multiple active sites, so it needs high temperature (450°C). The multiple active sites interaction with CO_2 is called as co-operative effect [39]. The cooperative effect is shown in Schemes S3 and S4. Moreover, the multi-molecular pillared mechanism is followed (Scheme S3), in which positive charges are appeared on oxygen atom, the charges are repel to each other through space and two negative charges are

appeared on the carbon are also helpful to relieve oxygen from carbon. These two factors reduced the decomposition temperature. Hence the reaction has been undergone at lower temperature compare to the conventional methods.

4.2 Innovative Concept of Catalysis

As heterogeneous catalysis is a surface phenomenon, the activity of heterogeneous catalyst depends upon the surface area of the catalyst. In other words, the rate of the reaction and the conversion are directly proportional to the catalyst surface area [40]. But in our catalyst, the conversion is not depending on surface area because surface area of our catalyst is very low, but conversion is high. This observation is against the well-known heterogeneous catalysis phenomenon. This factor induces us to invent the new concept which is involved in the reaction. In order to determine whether the reaction is surface area dependent or acidic/active sites dependent, we have to correlate the conversion and surface area which is as follow as.

Conversion (C) α Surface area (S)

$$C = K S \qquad (1)$$

$$K = \frac{C}{S}$$ where K is Conversion constant

We have applied this equation for CO_2 decomposition over the catalyst MgO-$AlPO_4$. In this catalytic process, the value of conversion and surface area are 99% and 59m^2/g respectively.

$$\text{So,} \qquad K = \frac{99}{59} = 1.6$$

It is assumed that If $K < 1$ it is depended on acidic/active sites of the catalyst

If $K > 1$ it is depended on the surface area of the catalyst

The CO_2 decomposition reaction has the K value is 1.6 over the MgO-$AlPO_4$ catalyst which is depended on the acidic / active sites. In order to find out the number of molecules assembling on an acidic / active site per minute for conversion, we need to correlate the conversion with temperature. So, we need the data for **rate constant** and **total active/ acidic sites** (concentration of acidity). These two values can be obtained from the intercept (rate constant) and slope (concentration of acidity) of the plot. By using these data, we have formulated a new formula for calculating the number of molecules assembling over acidic / active site per minute.

The formula is as follows.

Number of molecules assembling over an acidic / active site per minute, $$P_n = R\frac{mT}{W\,t} \quad (2)$$

where Pn – multimolecular Pillared assembling of CO_2 on acidic/active site
R- rate constant
m- active/acidic site concentration
T- temperature
W- weight of the catalyst
t- time

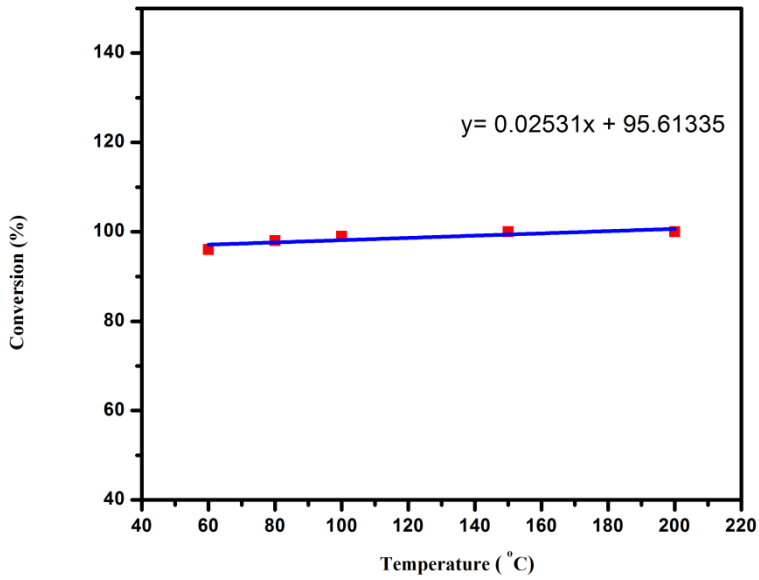

Figure 8. Acidic/ active site effect on CO_2 conversion over MgO-$AlPO_4$ catalyst

Multi-molecular pillared assembling of molecule on an active/acidic site per minute,

$$P_n = 95.61 \times \frac{0.025 \times 200}{1 \times 60}$$

$$= 8 \text{ molecules}$$

If more than two molecules assembling on active/acidic site, it may be consider as a CO_2 pillar. Now, we substitute the values, which are obtained from the Figure 8 in the equation -2, we have a result of 8 molecules assembling on active/acidic site per minute. So, it is a multi-molecular pillared assembling of CO_2. The same formula is applied for various catalysts for verifying its validity (Table S2). All catalysts have 'K' value more than 1 which is indicated that the CO_2 conversion reaction is depended on acidic / active sites. The catalysts which have positive value of 'm' is denoted that the acidic/active sites are active during the reaction, but the catalysts which have negative value of 'm' is denoted that the acidic/active sites are deactivated during the reaction (Table S2). The deactivation means that the conversion decreases with increased of temperature. So the multi-molecular assembling mechanism is not applicable for the catalyst with negative value of P_n.

4.3 Proposed Mechanism for the multi-molecular pillared decomposition of CO_2

The multi-molecular pillared decomposition means that many molecules are arranged one and above and formed a pillar like structure. The length of the pillar is depended on the acidic site affinity towards CO_2 molecule. The strength of the acidic sites depends on the metal ion and its co-ordination in the framework. The multi-molecular pillared assembling mechanism is shown in Scheme S3 and it is proposed based on the formula (2). As per the formula (2) 8 molecules of CO_2 assembling as a multimolecular pillar on two acidic sites. Then the pillar has positive charge on each oxygen atom and the positive charges are repelling themselves to break down the pillar to produce oxygen and olefinic carbon chain.

At the end of the reaction the olefinic chain is removed from the acidic sites. The olefinic carbon chain is an allene molecule with the ketonic group at both end (Scheme S3). It is a new molecule. Thus the carbon are captured from carbon dioxide and O_2 is released which is the important process for global warming reduction. This reaction is otherwise known as carbon capturing. This mechanism is supported by CO% (Table S2). If the catalyst is not followed the multi-molecular assembling mechanism, the CO production is high and also P_n is negative (Table S2). If the catalyst followed the multi-molecular assembling mechanism, it is produced less CO and high O_2%. So, these data are proved the multi-molecular pillared decomposition of CO_2.

4.4 UV-Visible Spectrum

The multimolecular pillared decomposition of CO_2 is confirmed by the formation of a new molecule of Octa-allene diketone. So we have characterized the catalyst after the reaction by UV-Vis spectrum. The UV–Vis spectrum of MgO-$AlPO_4$ after reaction is shown in the Figure 9 in order to confirm the presence of diketone product in the pores of the catalyst.

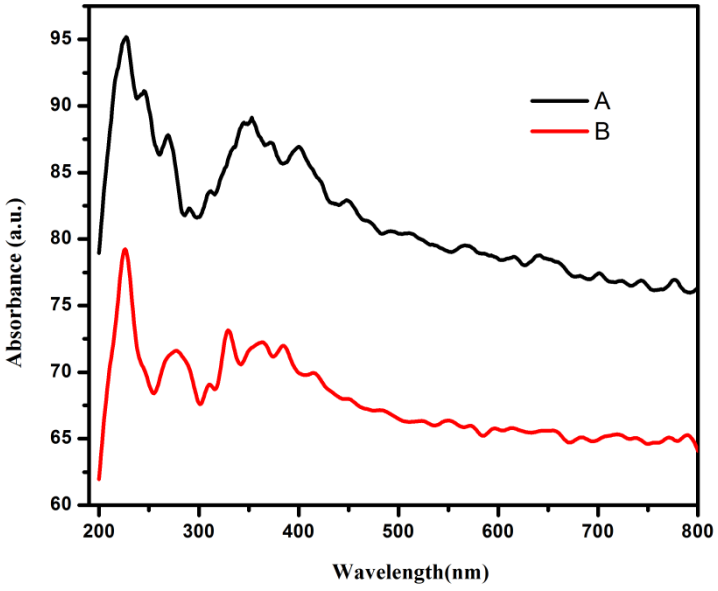

Figure 9. UV-Visible Spectra of MgO-$AlPO_4$ after the reaction (A) and water washed MgO-$AlPO_4$ after reaction (B)

The first band at 200-300nm may be due to the presence of diketone product (Scheme S3) [41][42].The second band is observed at 300-400 nm may be assigned to the presence of carbon nanoparticles [43][44]. But in the water washed MgO-$AlPO_4$ after reaction (B) spectrum, the intensity of the both bands are reduced. This means that many of the diketone and carbon nanoparticles are removed when the catalyst is washed with water.

4.5 Proposed Mechanism for the partial CO_2 decomposition

The multi-molecular pillared decomposition requires cooperation of two acidic sites (Scheme S3). But the non-pillared CO_2 decomposition needs only one acidic site. The non-pillared CO_2 decomposition is produced more CO molecules (Scheme S4). It is a partial decomposition. In this mechanism the CO_2 is vertically seated on a single acidic site. The intermediate has positive charge and it is neutralized by releasing the oxygen to produce CO. The mechanism of non-pillared CO_2 decomposition is shown in Scheme S4. Thus it is proved that two acidic sites cooperation is essential for complete decomposition of CO_2 to produce O_2 and capturing the carbon.

Conclusion

This study has revealed the intercrossing of two frameworks such as MgO and $AlPO_4$ for producing a novel framework with four types of acidic sites. This is characterized by XRD, FT-IR, BET, TGA and TEM analyses. The XRD pattern and crystal structure **proved that the two frameworks are intercrossed to form a novel framework material** (**Kankarlite-2**) and producing multiple active sites such as superoxide ion, oxyanion, octahedral Al^{3+} and Mg^{2+}. FT-IR is confirmed that the $AlPO_4$ is in both octahedral and tetrahedral framework and MgO is in octahedral framework. The BET analysis is confirmed

that the formation of double mesopores. The surface area is $59m^2/g$ and pore volume is 2.9 cm^3/g. Though the surface area and pore volume are less, the catalytic activity is too high due to the cooperative effect of active sites. The TGA and TEM analysis are confirmed that the intercrossing of two frameworks. The material is applied for CO_2 decomposition and it is observed that the CO_2 molecules are assembling as a **multimolecular pillar** and decomposed to release oxygen and produced a new molecule of **Octa allene diketone (C_8O_2)**. This decomposition is required two acidic sites cooperation and if the CO_2 seated on a single acidic site to produce CO and O. In this view, the superoxide ion, octahedral Al^{3+} and Mg^{2+} are having more than two acidic sites. So these acidic sites are responsible for complete decomposition (**multi-molecular pillared decomposition**). But the oxyanion is responsible for partial decomposition to CO. The fact is confirmed from the temperature effect of the reaction which produced around 75% of O_2 and 25% of CO. This means that the catalyst has 25% oxyanion and 75% of other three multiple active sites. The decomposition is depending on acidic sites but not depends on surface area which is proved by a new formula $\mathbf{P_n = R\frac{mT}{Wt}}$. The catalyst reduces the CO_2 decomposition temperature (63%) compared to the conventional methods. The intercrossing framework of MgO and $AlPO_4$ is an effective catalyst for CO_2 decomposition at lower temperature and the carbon is captured as a new **octa allene diketone** molecule.

References

1. Reddy MSB, Ponnamma D (2021) RSC Advances Carbon dioxide adsorption based on

porous materials. 12658–12681. https://doi.org/10.1039/d0ra10902a

2. Kargari A, Takht M (2012) Carbon Dioxide: Capturing and Utilization. Greenh Gases - Capturing, Util Reduct. https://doi.org/10.5772/33953

3. Boot-Handford ME, Abanades JC, Anthony EJ, et al (2014) Carbon capture and storage update. Energy Environ Sci 7:130–189. https://doi.org/10.1039/c3ee42350f

4. Haider MB, Hussain Z, Kumar R (2016) CO2 absorption and kinetic study in ionic liquid amine blends. J Mol Liq 224:1025–1031. https://doi.org/10.1016/j.molliq.2016.10.044

5. Ramdin M, De Loos TW, Vlugt TJH (2012) State-of-the-art of CO 2 capture with ionic liquids. Ind Eng Chem Res 51:8149–8177. https://doi.org/10.1021/ie3003705

6. Shaikh AR, Ashraf M, AlMayef T, et al (2020) Amino acid ionic liquids as potential candidates for CO2 capture: Combined density functional theory and molecular dynamics simulations. Chem Phys Lett 745:137239. https://doi.org/10.1016/j.cplett.2020.137239

7. Ma C, Wang N, Ye N, Ji X (2021) CO2 capture using ionic liquid-based hybrid solvents from experiment to process evaluation. Appl Energy 304:117767. https://doi.org/10.1016/j.apenergy.2021.117767

8. Liu Y, Dai Z, Zhang Z, et al (2021) Ionic liquids/deep eutectic solvents for CO2 capture: Reviewing and evaluating. Green Energy Environ 6:314–328. https://doi.org/10.1016/j.gee.2020.11.024

9. Gunasekaran P, Veawab A, Aroonwilas A (2013) Corrosivity of single and blended amines in CO2 capture process. Energy Procedia 37:2094–2099. https://doi.org/10.1016/j.egypro.2013.06.088

10. Zeng H, Qu X, Xu D, Luo Y (2022) Porous Adsorption Materials for Carbon Dioxide Capture in Industrial Flue Gas. Front Chem 10:1–18. https://doi.org/10.3389/fchem.2022.939701

11. Sheng N, Chu Y, Xin S, et al (2016) Insights of the Crystallization Process of Molecular Sieve AlPO4-5 Prepared by Solvent-Free Synthesis. J Am Chem Soc

138:6171–6176. https://doi.org/10.1021/jacs.6b01200

12. Bandyopadhyay M, Bandyopadhyay R, Kubota Y, Sugi Y (2000) Synthesis of AlPO4-5 and AlPO4-11 molecular sieves by dry-gel conversion method. Chem Lett 1024–1025. https://doi.org/10.1246/cl.2000.1024

13. Pathak LC, Singh TB, Das SK (2004) Role of templating agents on the growth morphology of AlPO4. J Mater Sci 39:4069–4071. https://doi.org/10.1023/B:JMSC.0000031498.85640.43

14. Li D, Yao J, Wang H (2012) Hydrothermal synthesis of AlPO4-5: Effect of precursor gel preparation on the morphology of crystals. Prog Nat Sci Mater Int 22:684–692. https://doi.org/10.1016/j.pnsc.2012.11.003

15. Karthika Devi K, Chellapandiankannan (2022) Metal ion effect on pore enlargement in solid acid catalyst and CO2 decomposition. J Porous Mater. https://doi.org/10.1007/s10934-022-01399-8

16. Karthik M, Vinu A, Tripathi AK, et al (2004) Synthesis , characterization and catalytic performance of Mg and Co substituted mesoporous aluminophosphates. 70:15–25. https://doi.org/10.1016/j.micromeso.2004.02.012

17. Mangamma G, Ajikumar PK, Kamruddin M, et al (2011) Synthesis and characterization of nanocrystalline CrN. Adv Sci Lett 4:622–626. https://doi.org/10.1166/asl.2011.1263

18. Gutierrez-Puebla E (2016) Interlacing molecular threads. Science (80-) 351:336–336. https://doi.org/10.1126/science.aad9671

19. Chambron JC, Dietrich-Buchecker C, Hemmert C, et al (1990) Interlacing molecular threads on transition metals. Pure Appl Chem 62:1027–1034. https://doi.org/10.1351/pac199062061027

20. Pu Y, Wu W, Liu J, et al (2018) A defective MOF architecture threaded by interlaced carbon nanotubes for high-cycling lithium-sulfur batteries. RSC Adv 8:18604–18612. https://doi.org/10.1039/c8ra02254b

21. Hunziker EB, Straub PW, Haeberli A (1990) A new concept of fibrin formation based

upon the linear growth of interlacing and branching polymers and molecular alignment into interlocked single-stranded segments. J Biol Chem 265:7455–7463. https://doi.org/10.1016/s0021-9258(19)39135-5

22. S. Siva Sankari SSS, M. A. Mary Thangam MAMT, Chellapandian Kannan CK (2019) Carbon Dioxide Decomposition Over AlPO4 Based Molecular Sieves. J Environ Nanotechnol 8:25–33. https://doi.org/10.13074/jent.2019.03.191345

23. Feng L, Qi X, Li Z, et al (2009) Synthesis and characterization of magnesium-substituted aluminophosphate molecular sieves (MgAPO-11) and their kinetic study of catalytic cracking of n-hexane. Cuihua Xuebao / Chinese J Catal 30:340–346. https://doi.org/10.1016/s1872-2067(08)60101-1

24. Zahir MH, Rahman MM, Irshad K, Rahman MM (2019) Shape-stabilized phase change materials for solar energy storage: MgO and mg(OH)2 mixed with polyethylene glycol. Nanomaterials 9:1–21. https://doi.org/10.3390/nano9121773

25. Zhai JP, Tang ZK, Li ZM, et al (2006) Carbonization mechanism of tetrapropylammonium-hydroxide in channels of AlPO4-5 single crystals. Chem Mater 18:1505–1511. https://doi.org/10.1021/cm0526821

26. Umamaheswari V, Kannan C, Mathiarabindoo B, et al (2000) Isomorphous substitution of Mn(II), Ni(II) and Zn(II) in A1PO-31 molecular sieves and study of their catalytic performance. Proc Indian Acad Sci Chem Sci 112:439–448. https://doi.org/10.1007/BF02704349

27. Nassar MY, Ahmed IS, Samir I (2014) A novel synthetic route for magnesium aluminate (MgAl 2 O 4) particles using sol-gel auto combustion method and their photocatalytic properties Mostafa Y . Nassar , Ibrahim S . Ahmed *, Ihab Samir Abstract In this paper a novel and inexpensive route for. Spectrochim ACTA PART A Mol Biomol Spectrosc. https://doi.org/10.1016/j.saa.2014.04.040

28. Salman KD, Abbas HH, Aljawad HA (2021) Synthesis and characterization of MgO nanoparticle via microwave and sol-gel methods. J Phys Conf Ser 1973:. https://doi.org/10.1088/1742-6596/1973/1/012104

29. Papageorgiou A, Reddy KSK, Karonis D, et al (2020) Morphology, Activation, and

Metal Substitution Effects of AlPO4-5 for CO2 Pressure Swing Adsorption. Front Chem 8:1–18. https://doi.org/10.3389/fchem.2020.568669

30. Eswaramoorthy M, Neeraj S, Rao CNR (1999) Synthesis of hexagonal microporous silica and aluminophosphate by supramolecular templating of a short-chain amine. Microporous Mesoporous Mater 28:205–210. https://doi.org/10.1016/S1387-1811(98)00309-6

31. Wang Y, Du T, Song Y, et al (2017) Amine-functionalized mesoporous ZSM-5 zeolite adsorbents for carbon dioxide capture. Solid State Sci 73:27–35. https://doi.org/10.1016/j.solidstatesciences.2017.09.004

32. Ren H, Xin F (2006) In situ calcinations of precursors of mesoporous AlPO4 and application of mesoporous Mn-AlPO4. Catal Commun 7:848–854. https://doi.org/10.1016/j.catcom.2006.03.010

33. Krishnaveni M, Kannan C (2021) A new mechanism for pore enlargement in mesoporous materials and its application on biodiesel production. Energy Sources, Part A Recover Util Environ Eff 00:1–16. https://doi.org/10.1080/15567036.2021.1987587

34. Masson NC, Pastore HO (2001) Synthesis and characterization of tubular aluminophosphate mesoporous materias containing framework magnesium. Microporous Mesoporous Mater 44–45:173–183. https://doi.org/10.1016/S1387-1811(01)00182-2

35. Diaz I, Mayoral A (2011) TEM studies of zeolites and ordered mesoporous materials. Micron 42:512–527. https://doi.org/10.1016/j.micron.2010.12.005

36. Pomytkin AP, Words-oxidation K (1993) HIGH-TEMPERATURE OXIDATION BEHAVIOUR. 31:

37. Zhang K, Harvey AP (2021) CO2 decomposition to CO in the presence of up to 50% O2 using a non-thermal plasma at atmospheric temperature and pressure. Chem Eng J 405:126625. https://doi.org/10.1016/j.cej.2020.126625

38. Bajaj NK, Periasamy S, Singh R, et al (2021) The catalytic decomposition of carbon dioxide on zinc-exchanged Y-zeolite at low temperatures. J Chem Technol Biotechnol 96:2675–2680. https://doi.org/10.1002/jctb.6815

39. Uuniversity A (1998) Hydration of ethylene in the vapour phase over N A P O - 5 and ZAPO-5. 110:491–497

40. Bernard P, Stelmachowski P, Broś P, et al (2021) Demonstration of the Influence of Specific Surface Area on Reaction Rate in Heterogeneous Catalysis. J Chem Educ 98:935–940. https://doi.org/10.1021/acs.jchemed.0c01101

41. Zhang J, Wang S, Lalevée J, et al (2020) 1 , 2-Diketones as Photoinitiators of both Cationic and Free-Radical Photopolymerization under UV (392 nm) or Blue (455 nm) LEDs. 1–11. https://doi.org/10.1002/pol.20190157

42. Sai L, Jiao S, Yang J (2020) Ultraviolet Carbon Nanodots Providing a Dual-Mode Spectral Matching Platform for Synergistic

43. Murugan K, Nataraj D, Madhiyazhagan P, et al (2015) Carbon and silver nanoparticles in the fight against the filariasis vector Culex quinquefasciatus : genotoxicity and impact on behavioral traits of non-target aquatic organisms. https://doi.org/10.1007/s00436-015-4837-9

44. Sh MS, Fard FG, Khatibi E, Sarpoolaky H (2009) Journal of the Taiwan Institute of Chemical Engineers Dispersion and stability of carbon black nanoparticles , studied by ultraviolet – visible spectroscopy. 40:524–527. https://doi.org/10.1016/j.jtice.2009.03.006